Journal of Sol-Gel Science and Technology (2024) 110:169–182
https://doi.org/10.1007/s10971-024-06350-8

ORIGINAL PAPER

Investigation of the effect of graphene oxide nanoparticles on the structural and dielectric parameters in zinc oxide semiconductors

Merve Horlu[1] · Cevher Kursat Macit[2] · Bunyamin Aksakal[2] · Burak Tanyeri[2] · Fatih Biryan[3]

Received: 18 December 2023 / Accepted: 18 February 2024 / Published online: 6 March 2024

Abstract

In this study, pure and 1%, 3% and 5% doped graphene oxide (GO) reinforced zinc oxide (ZnO) nanoparticles were synthesized by sol-gel method. The aim was to improve the electrical and dielectric properties of ZnO semiconductor metal oxide used in many electronic, optoelectronic and electrochemical technologies. FE-SEM, X-ray diffraction (XRD), Raman spectroscopy, energy dispersive spectroscopy and Fourier transform infrared spectroscopy (FT-IR), were used to show the structural and morphological properties of the synthesized ZnO and GO doped ZnO nanoparticles. Impedance analysis was used to study the dielectric properties of the produced nanoparticles. XRD analysis revealed typical peaks of nGO and ZnO nanoparticles. Through the FE-SEM and XRD analysis, it was shown that the ZnO and GO nanopowders were successfully synthesized. The results revealed that ZnO-GO nanoparticles, having good dielectric constant with loss and AC conductivity values, such materials can be a good candidate for solar cells and photovoltaic devices.

Graphical Abstract

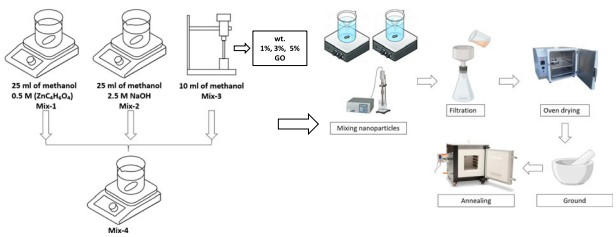

Keywords Nanomaterial · Sol-gel · Semiconductor · Graphene oxide doped zinc oxide · Conductivity

Highlights

- GO reinforced ZnO nanoparticles with high purity and homogeneity were produced by sol-gel synthesis.
- Structural and morphological analyses revealed that GO nanoparticles were incorporated into ZnO nanoparticles and retained their characteristic peaks.
- According to FE-SEM images, ZnO nanoparticles and GO nanoparticles were homogeneously dispersed on the surface of ZnO nanorods and plates. The crystal diameters, unit cell volume and lattice properties of the nanoparticles increased with increasing GO addition.
- The addition of GO to ZnO nanoparticles improved their dielectric response and the addition of GO to the electrical conductivity had a positive effect on ZnO nanoparticles.

✉ Cevher Kursat Macit
macitkursatcevher@gmail.com

[1] Firat University, Technology Faculty, Department of Mechanical Engineering, 23119 Elazig, Turkey

[2] Firat University, School of Aviation, Aircraft Airframe-Engine Maintenance, 23119 Elazig, Turkey

[3] Firat University, Faculty of Science, Department of Chemistry, 23119 Elazig, Turkey

1 Introduction

With the recent developments in nanotechnology and nanoscience, it is evident that the utilization areas of diverse nanostructured materials with applications in electronics, energy storage, pharmacy, and medical sciences are rising and the research continue to grow day by day [1]. Transition metals, silicon, carbon, and metal oxides are the most commonly employed nanoparticles (NPs) in application sectors. Metal oxide NPs are of particular interest among NPs due to their distinct physical and chemical characteristics [2–4]. Metal oxide nanoparticles (NPs) are currently generating a lot of scientific buzz due to their many prospective uses in biological, optical, and electronic sectors. Zinc oxide (ZnO), titanium dioxide (TiO2), copper oxide (CuO), zirconium dioxide (ZrO2), aluminum oxide (Al2O) 3, silicon dioxide (SiO2), iron oxide (Fe3O4), magnesium oxide (MgO), nickel oxide (NiO), manganese dioxide (MnO2), and other materials can be used to develop metal oxide nanoparticles [4, 5].

Semiconductor metal oxides, which are widely used in new electronic, magnetic, dielectric, and optical applications in metal oxide structures, are of great research interest [6]. Bonding multiple metal oxides has a profound effect on the electrical structure at the combined metal-oxide interfaces and is expected to improve other physical properties. Semiconductor metal oxides with low dielectric loss and high dielectric constants are useful in microelectronics, semiconductor devices, sensors, electrochemical devices, optoelectronic devices, nonvolatile memory storage devices, and fuel cells, among other applications [7–11]. Dielectric and alternating current (AC) conductivity tests analyze the uniqueness of producing a semiconductor metal oxide device, and these measurements are required to identify the presence of structural-related flaws in the material and to analyze the conduction process [12].

The n-type semiconductor used as the study's matrix material, ZnO nanoparticles, is widely researched and manufactured for use in solar cells, gas sensors, transistors, chemical absorbers, electrical and optical devices, liquid phase hydrogenation catalysts, and photocatalytic degradation catalysts [13]. As a result, having many advantages, there exist a lot of interest in studying the fabrication and manipulation of nanoscale ZnO structures. It is a substantial semiconductor first and foremost, with a big band gap of 3.37 eV and a high binding energy of 60 meV. Second, it plays a significant role in the creation of piezoelectric sensors and transducers that are coupled with electromechanical systems. ZnO can be applied directly in biological applications and due to its distinctive features, ZnO structures have emerged as one of the most significant nanomaterials in research and application studies [14]. For foundational studies, many techniques have been employed to generate nanostructured ZnO powders with varied morphologies and ionic dopants [15–23]. Graphene has been one of the most investigated materials over the last 30 years due to its remarkable properties, such as its high specific surface area, mechanical flexibility, thermal conductivity, distinctive optical features, strong electrical conductivity, and rapid charge carrier mobility [24–27].

Because of their numerous promising performances in device applications, graphene, and graphene-based materials have attracted the scientific community's curiosity, and this enthusiasm appears to be growing [28, 29]. Graphene oxide (GO), a form of graphene, is a highly specialized material primarily due to its distinctive structure and remarkable properties [28, 29]. The oxygen-containing group in GO gives it an important interaction with other materials. Hybridization structures of localized sp^2 GO support carrier migration to some extent. GO exhibits excellent application areas for dielectric composites in areas in the insulated state. Due to dielectric composites' polarization and loss mechanisms, GO has a wide range of applications in this context [30]. Nanoparticles of graphene-metal oxide nanocomposites have been studied to improve dielectric, optical, and electrical properties. Graphene oxide (GO), reduced graphene oxide (RGO), and functionalized graphene oxide (FGO) have been demonstrated to increase their electrical, optical, and electrical properties when mixed with other materials such as ceramics, metal oxide, and polymers [5, 6, 30]. Due to these properties, it has many potential applications as a material in multifunctional electronic and optoelectronic devices [3, 4, 24–29].

A review of the literature on the fabrication of GO-doped ZnO nanoparticles shows that GO addition effectively prevents the aggregation of ZnO particles and provides strong stability in the medium. The large surface area of GO and the wide bandgap of ZnO particles significantly enhance the electrochemical properties of ZnO/GO composites compared to pure ZnO particles and graphene oxide alone, and may increase the application area of ZnO nanoparticles [31–35].

It is commonly acknowledged that nanoparticles can be produced chemically or physically. Sol-gel processing, electrochemical procedures, hydrothermal techniques, and chemical vapor deposition are examples of these processes. Larger specific surface area, superior homogeneity and purity, better microstructure control for metallic particles, smaller pores and uniform particle distribution, ease of manufacture, low cost, reproducibility, and homogeneous nanoparticle production are the main benefits of sol-gel processing over conventional methods [36, 37].

In this study, ZnO nanoparticles, whose dielectric properties have not been investigated, were produced using sol-gel method by reinforcing GO nanoparticles at 1 wt.%, 3 wt.% and 5 wt.%. The main objective of this study is to improve the electrical and dielectric properties of ZnO semiconductor metal oxide, which can effectively be used

in many electronic, optoelectronic and electrochemical technologies. XRD, FT-IR, Raman, FE-SEM, and EDX analyses were used to describe the structural and morphological properties of the synthesized nanoparticles. The structural and morphological properties of newly fabricated nanoparticles, as well as their interaction with dielectric properties, were comprehensively examined and analyzed.

2 Materials and method

2.1 Nanoparticle synthesis

The production of pure ZnO and GO-doped ZnO nanoparticles used in the study by sol-gel synthesis method was started by adding 0.5 M ($Zn(CH_3COO)_2 2H_2O$) into 25 ml methanol in a beaker and stirring. The mixture was stirred on a magnetic stirrer (Mix-1) until dissolved. In another beaker, 2.5 M NaOH was added to 25 ml of methanol and swirled until dissolved with a magnetic stirrer. (Mixture-2). These two solutions were mixed in a beaker and another 10 ml of methanol was added to the mixture (Mixture-3). The completed solution was agitated in a magnetic stirrer at 90 °C for four hours. After stirring, the solution was allowed to reach room temperature. The nanoparticles were then filtered with filter paper and washed with alcohol. After cleansing with alcohol, the solution was rinsed several times with distilled water before being annealed in an oven at 450 °C for an hour and crushed with a crusher and pestle. Thus, pure ZnO nanoparticles were produced as sample 1, and the same process steps were repeated to produce ZnO nanoparticles with GO addition. The only modification made was that the nano-GO particles were added to 20 ml of methanol in weight percentages (10, 20, 30%) and then blended in another beaker using an ultrasonic homogenizer (Mix-4) for 30 min. Mix-4 was then added to Mix-3 and all the procedures to obtain pure ZnO were repeated. The nanoparticle synthesis flow chart and sol-gel production scheme are shown in Fig. 1 and the nomenclature with additive amounts of the nanoparticles produced are given in Table 1.

2.2 ZnO-GO nanoparticle morphological characterization

The functional groups of pure and GO-doped ZnO nanoparticles synthesized by the sol-gel method were characterized using FT-IR measurements (Thermo Scientific Nicolet IS5). The analysis was performed using a FT-IR spectrometer with a scanning range of 4000–500 cm^{-1}, and XRD (PANalytical Empyrean) of fabricated nanoparticles were obtained at CuKa (=1.5406 A) radiation at 40 kV/40 mA in the scanning range 2 = 10 to 80°. A Raman spectrometer system (WITech alpha 300 R) with excitation wavelengths of 532 and 325 nm, respectively, was used to produce nonresonant and RRS results. FE-SEM (Zeiss Sigma 300) and EDX analyses were used to analyze the form and chemical content of the nanoparticles, as well as particle sizes and degree of doping.

2.3 ZnO-GO nanoparticle dielectric measurements

Using an impedance analyzer (HIOKI, Japan) with a frequency range of 1000 Hz to 2000000 Hz, the dielectric properties of the produced ZnO-GO nanoparticles were examined. The disc thicknesses were precisely measured with a digital caliper after the powder samples were initially pelletized under a 10-ton pressure. At room temperature, measurements of conductivity (Gp), loss factor (DF), and capacitance (Cp) were made on discs of a 13 mm diameter. Between the two capacitors, samples were consecutively collected, and in the impedance analyzer's electric field region, dielectric parameters were calculated.

3 Results and discussion

3.1 XRD of ZnO-GO nanoparticles

Figure 2 shows XRD diffraction patterns of pure and GO-doped ZnO nanoparticles manufactured in various ratios. Tables 2 and 3 provide the two values and estimated values of diffraction planes, respectively, providing the lattice sizes, unit cell volumes, crystal and average crystal sizes. The crystal sizes of the samples were determined using the high-density (101) peak, and the structural parameters were determined using Bragg's formulae. The Debye-Scherrer equation is employed in Eq. (1) to calculate the average crystal size of the nanoparticles [38–40].

$$D = \frac{0.9\lambda}{B\cos\theta_B} \tag{1}$$

where the full width at half maximum is measured in radians, the diffraction angle is measured in degrees, and the X-ray wavelength is computed in nanometers. The distance (d) between two adjacent planes can be determined using Eq. (2) [34].

$$\frac{1}{d^2} = \frac{4}{3}\left(\frac{h^2 + hk^2 + k^2}{a^2}\right) + \frac{I^2}{c^2} \tag{2}$$

where the Miller indices are h, k, and l and d stands for the distance between two nearby planes. Using Eq. (3), the volumes of the unit cells (V) were computed [37–39].

$$V = \frac{\sqrt{3}}{2}a^2c = 0.866\,a^2c \tag{3}$$

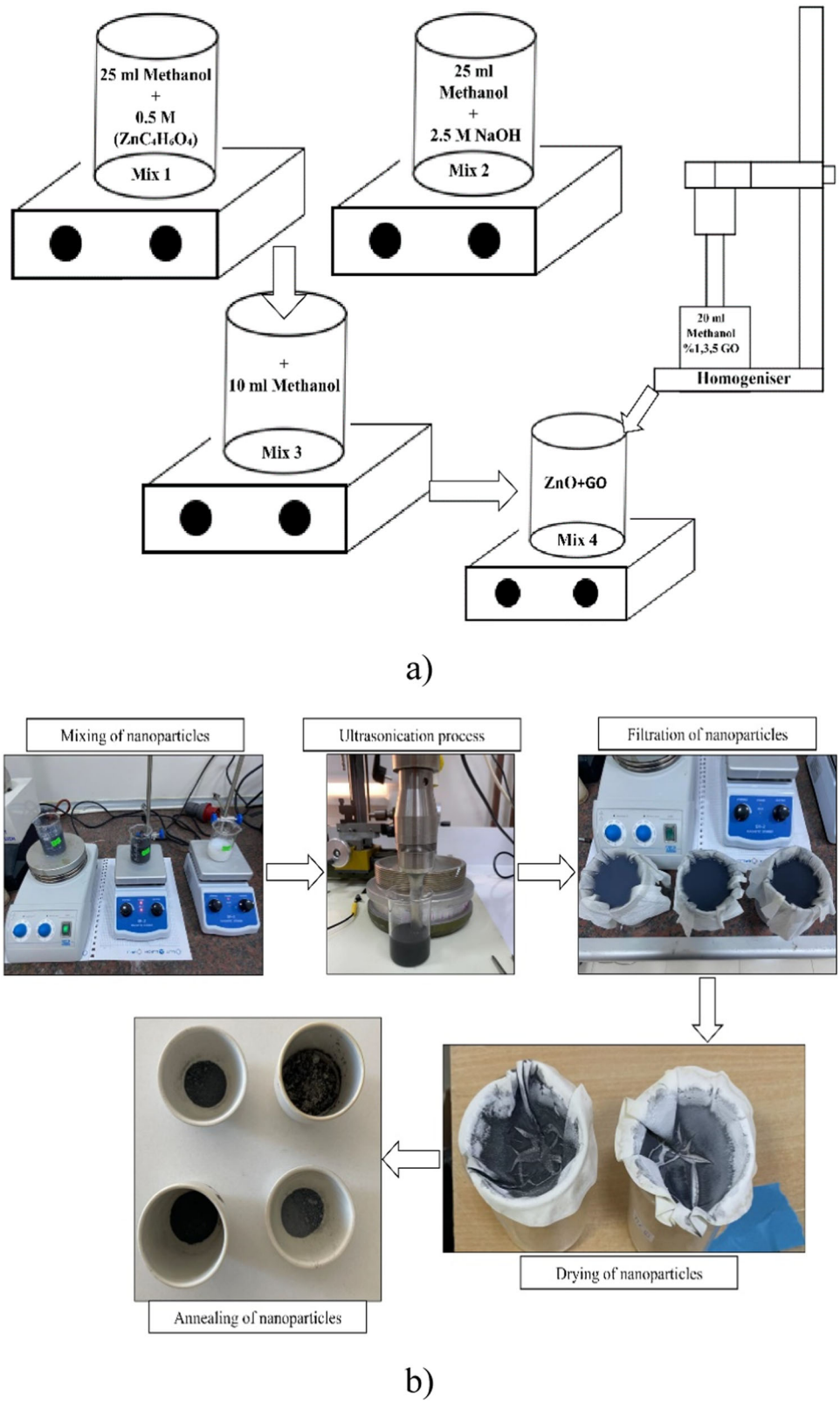

Fig. 1 **a** Preparation of mixtures. **b** Preparation of nanoparticles

The intense peaks corresponding to 31.913°, 34.541°, 36.345°, 47.605°, 56.642°, 62.893°, 66.430°, 68.003°, 69.115°, 72.536°, 77.055° 2θ degrees in pure ZnO sample are consistent with JCPDS card 36-1451 and these peaks are characteristic peaks of ZnO [41, 42]. Planes (100), (002), (101), (102), (110), (103), (200), (112), (201), (004), and

Table 1 Nomenclature and additive amounts of synthesized nanoparticles

Sample	Content
ZnO	100% ZnO
GO	100% GO
ZnO-1GO	1 wt% GO, 99% ZnO
ZnO-3GO	3 wt% GO, 97% ZnO
ZnO-5GO	5 wt% GO, 95% ZnO

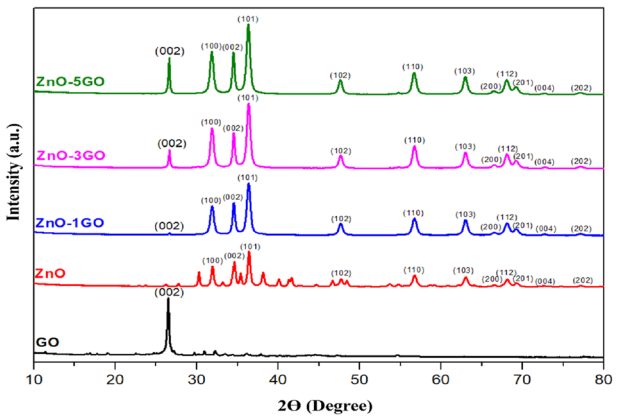

Fig. 2 XRD diffraction patterns of the synthesized nanoparticles

(202) correspond to these peaks [42, 43]. These characteristic peaks of ZnO are indexed to the hexagonal Wurtzite structure. In addition to the characteristic peaks of pure ZnO in the nanoparticles, the characteristic carbon peak of GO is observed at 26.514° 2θ and this peak corresponds to the (002) plane [44–46]. It is observed that the peak intensities in the (002) plane increase as the GO doping ratio increases and the shifts occur when combined with ZnO.

The lattice dimensions with corresponding lattice parameters calculated using Eqs. (1)–(3) were found to be very close to the lattice dimensions of the pure ZnO given in Table 3). The size of the crystallites was observed that the lattice parameters and unit cell volume decreased when ZnO was combined with GO, and XRD peaks shifted to higher angles [47]. With the addition of graphene oxide nanosheets, this decreasing behavior in lattice constants is thought to have occurred due to local lattice disorder or strain generation, evidencing the presence of empty lattice sites and the decreasing nature of the average crystallite size. The decrease in lattice parameters of GO-doped ZnO nanoparticles indicates the further reduction that may result from the aggregation of GO nanorods by the ZnO matrix. Moreover, this decreasing behavior in the lattice constants may have occurred due to local lattice disorder or strain formation, which evidences the presence of empty lattice sites and the

Table 2 Two diffraction plane values of the synthesized nanoparticles

Sample/ Diffraction plane	GO	ZnO	ZnO-1GO	ZnO-3GO	ZnO-5GO
(002) GO	**26.514**	–	**26.659**	**26.673**	**26.687**
(100)	–	31.913	31.928	31.942	31.957
(002)	–	34.541	34.570	34.598	34.613
(101)	–	36.345	36.360	36.388	36.403
(102)	–	47.605	47.620	47.648	47.663
(110)	–	56.642	56.685	56.714	56.743
(103)	–	62.893	62.936	62.965	62.979
(200)	–	66.430	66.444	66.487	66.502
(112)	–	68.003	68.047	68.061	68.090
(201)	–	69.115	69.187	69.216	69.245
(004)	–	72.536	72.579	72.652	72.666
(202)	–	77.055	77.069	77.112	77.127

Table 3 The calculated a = b, c, V and crystalline size values of synthesized nanoparticles [71]

Sample	2 theta (101)	a (Å)	c (Å)	V (Å^3)	Crystallite size (nm)
ZnO	36.345	3,228	5.271	47.575	18.953
ZnO-1GO	36.360	3.226	5.269	47.518	16.512
ZnO-3GO	36.388	3.224	5.265	47.412	16.477
ZnO-5GO	36.403	3.223	5.263	47.356	16.467

decreasing nature of the average crystallite size [43]. Compared to pure ZnO, GO/ZnO nanoparticles showed a decrease in crystallite size with increasing GO concentration, which is related to the inhibition of the growth of ZnO nanoparticles by the presence of GO. The average crystallite size of the GO reinforced ZnO nanocomposites is found to be larger than that of pure ZnO [32, 48].

From the literature studies, the lattice parameters were found to be decreased as a result of different doping of ZnO nanoparticles [49]. It has been found that as the amount of GO reinforcement in ZnO nanoparticles increases, the crystallite size decreases. In the syntheses made by adding different reinforcement amounts to ZnO nanoparticles, it was observed that decreases in the lattice parameters of ZnO occurred. The changes and the reinforcements used are shown in Table 4.

3.2 FT-IR analyses of ZnO-GO nanoparticles

The FT-IR spectra of ZnO particles with GO added are shown in Fig. 3. Peaks at 383 cm^{-1}, 407 cm^{-1}, 480 cm^{-1}, 512 cm^{-1}, and 582 cm^{-1} in the FT-IR study correlate to Zn-O bonding [50, 51]. The 886 cm^{-1} vibrational mode is

Table 4 Effect of doping different nanoparticles in ZnO nanoparticles

Content	Synthesizing Method	Conclusion	Reference
Ag-ZnO	Green combustion with natural fuels	The lattice parameters of ZnO nanoparticles increased with Ag doping.	[53]
Ce-ZnO	Chemical precipitation	The lattice parameters of ZnO nanoparticles decreased with Ce doping.	[54]
Co-ZnO	Gel burning	The lattice parameters of ZnO nanoparticles increased with Co doping.	[55]
Cu-Mn-ZnO	The solid-state reaction method	Mn reinforcement up to 3 wt.% increased the lattice parameters. At 4 and 5, the lattice parameters started to decrease.	[56]
ZnO-TiC	Sol-gel	It was observed that the cage parameters also increased with increasing TiC carbide reinforcement.	[61]

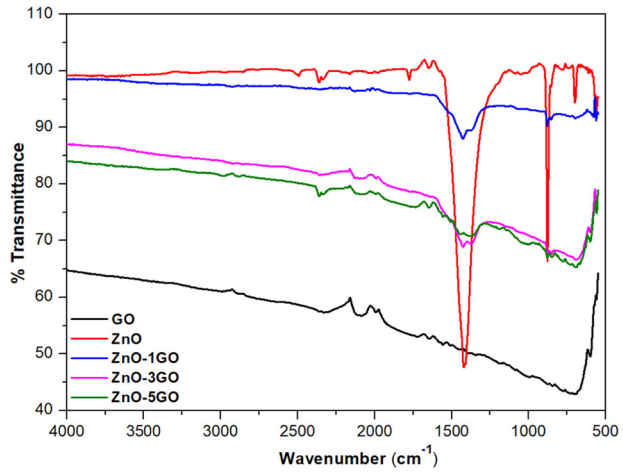

Fig. 3 FT-IR spectra of the nanoparticles

associated to substituted hydrogen in the oxygen region (HO) bound to the lattice Zn region (i.e., Zn-HO). These peaks correspond to the polar stretch vibration modes A1 (TO), E1 (TO), A1 (LO), and E1 (LO), respectively, for ZnO nanoparticles [50, 51].

The peak at 1066 cm^{-1} in the GO spectra displayed in Fig. 4 is attributable to C-O stretching. C-O-C bending is confirmed at 1288 cm^{-1}, while C-OH bending is seen at 1587 cm^{-1}. Carbonyl groups are also shown at 1724 cm^{-1} as C=O stretching, and a large peak at 3448 cm^{-1} is attributable to the C-OH groups' O-H stretching vibration and the material's water content [52–54]. In the FT-IR spectra, the O-H, C=O and C-O vibrational bands were found to be severely reduced, weakened and slightly shifted to a lower wave number due to deoxygenation in GO. The difference in morphology provides a chemical shift due to the arrangement of atoms in the structure, which produces a different response in the change of the dipole moment when the material interacts with infrared radiation [31–35].

3.3 Raman spectroscopy of ZnO-GO nanoparticles

Raman scattering is a sensitive and non-destructive characterization technique used to investigate the vibrational characteristics of materials with nanostructures, as well as to define the nature and structure of ZnO nanoparticles. Wurtzite-type ZnO is a member of the C^4_{6v} (P63mc) space group and has two formula units in the primitive cell. At the Brillouin zone point, the zone-center optical phonons exhibit irreducible representation: Γ opt $= 1A_1 + 2B_1 + 2E_1 + 2E_2$ [55, 56]. A1 and E1 are long-range electrostatic force polar modes, while B1 modes are Raman quiet modes. A1 and E1 are long-range electrostatic force polar modes, while B1 modes are Raman quiet modes [57, 58]. They are categorized as either longitudinal optical (LO) or transverse optical (TO) phonons. There are two frequencies in a nonpolar phonon mode with symmetry E2. The values of E2H and E2L, which correspond to oxygen atoms and the Zn sublattice, and A1, E1, and E2 are the active Raman modes [59, 60]. The weak peaks observed at about 307 and 603 cm^{-1} are driven by the transverse optical (TO) phonon mode emerging from the silicon substrate [61]. The second-order Raman (E2H) mode, which is characteristic of hexagonal wurtzite ZnO, is attributed to the peak at 432 cm^{-1}. Two novel modes at 494 and 707 cm^{-1} in the ZnO Raman spectra were found, and they were attributed to surface optical (SO) phonon modes [62].

Figure 4 shows the GO nanoparticles' Raman spectrum. The D and G bands are represented by two separate peaks in the 1000–2000 cm^{-1} area in the Raman spectra of GO. Graphene oxide shows two strong syndromic peak-to-peak modes, the G band at 1800–1900 cm^{-1} and the D band at 1250–1300 cm^{-1}. The G band indicates that there are all sp^2 hybrids in a two-dimensional hexagonal junction. As a result, a flawless crystal should not exhibit the D band, and Bahrami et al. saw a similar reflection in their research [62].

3.4 FE-SEM and EDX analyses of ZnO-GO nanoparticles

SEM pictures of synthesized GO-doped ZnO nanoparticles in various sizes are shown in Fig. 5, Fig. 6 shows EDX analysis results, and Table 5 shows the weight contribution amounts of the elements in the EDX analysis results. According to SEM views, the particles are observed to be in

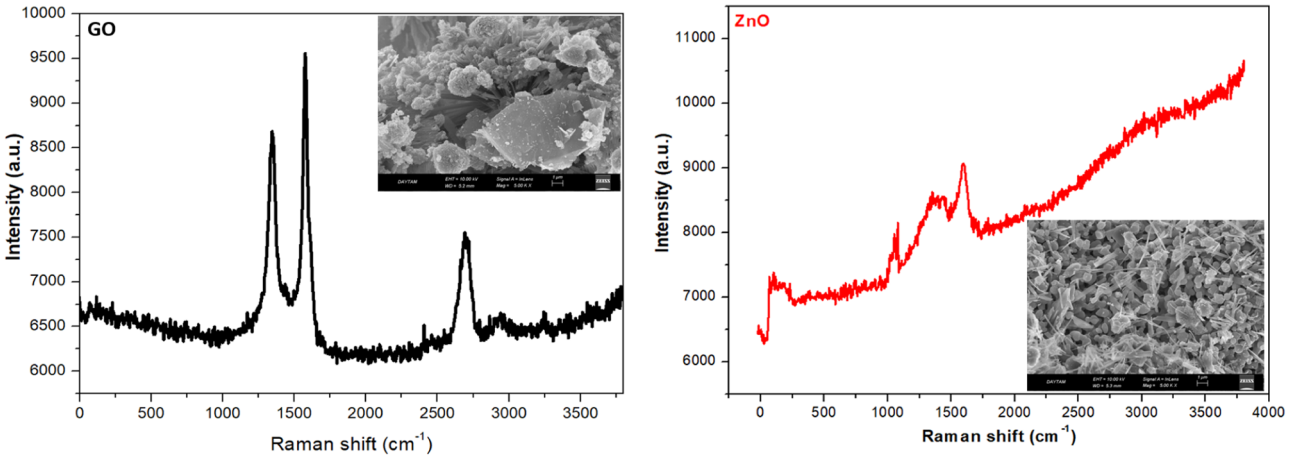

Fig. 4 Raman spectroscopy of the synthesized nanoparticles

nano-sized, and the GO nanoparticles are equally distributed on ZnO nanorods and plates. SEM images revealed that ZnO-GO particles were produced in nano size. Zn, O, and C elements were detected in the EDX spectra. Because GO has a higher molecular weight than the other materials used, an excess amount was formed in the EDX results, and an increase in the amount of C occurred as the amount of GO rose (Table 6).

The FE-SEM images show that the thickness of the hexagonal plates decreases, while the average thickness of the ZnO nanoparticles is slightly higher than that of the GO reinforced nanoparticles due to the strong agglomeration and clustering of pure ZnO nanoparticles. The nanoparticles were found to be in an agglomerated form, which could depend on the calcination temperature. There is less particle aggregation and agglomeration in the nanocomposite as the ZnO nanoparticles bind to GO by interacting with residual functional groups of GO basal planes. Increasing the amount of GO does not affect the morphology of pure ZnO but slightly reduces the average thickness of ZnO nanoparticles in GO/ZnO nanocomposites. From the micrograph of GO/ZnO nanocomposites, it is observed that ZnO nanoparticles are continuously dispersed on the GO sheets and accordingly the clarity of GO sheets in the nanoparticle decreases [63–68].

GO nanoparticles retain the original graphite's layered structure; however, they have a very heterogeneous size and shape distribution, with some particles much larger than others, as well as lamellae with defects caused by the oxidation process, as evidenced by the irregular ends of the sheets and lumps. GO exhibits greater delamination, as seen with thinner stacking of nanosheets. The ultrasonication technique at the margins has made the structures almost transparent to electron beams. FE-SEM pictures reveal that the nanoparticles transition from a regular, layered arrangement to an asymmetric structure of varying sizes with a rough and discontinuous morphology of the layers. This morphology is associated with the application of ultrasound. The migration of ultrasound waves through the dispersed material in liquid media is thought to lead to the formation of bubbles, which collapse when their volume increases, releasing a large amount of energy that can break down the material structure [31, 32].

3.5 Investigation of dielectric properties of ZnO-GO nanoparticles

To determine the dielectric properties of the ZnO-GO nanoparticles, the samples were first formed into discs with a diameter of 13 mm under 10 tons of pressure.. By using a digital caliper with an accuracy of 0.001 mm to measure the thickness of the pellets, the surface area was determined. Using a computer-controlled HIOKI brand IM3536 impedance analyzer, measurements for capacitance (Cp), loss factor (DF), and conductivity (Gp) were measured from 1 kHz to 200 kHz. The following equations were used to compute the conductivity (log ac), dielectric constant (ε‘), and dielectric loss (ε“) values based on the data attained. Figures 7–9 displays the nanoparticles' dielectric characteristics.

$$\varepsilon' = C_p \frac{d}{A\varepsilon_0} \tag{4}$$

$$\varepsilon'' = \varepsilon' DF \tag{5}$$

$$\sigma = G_p \frac{d}{A} \tag{6}$$

Three essential factors—ionic, electronic, and orientation—contribute to a given material's dielectric constant. One of the aspects of contribution, the orientations, result from

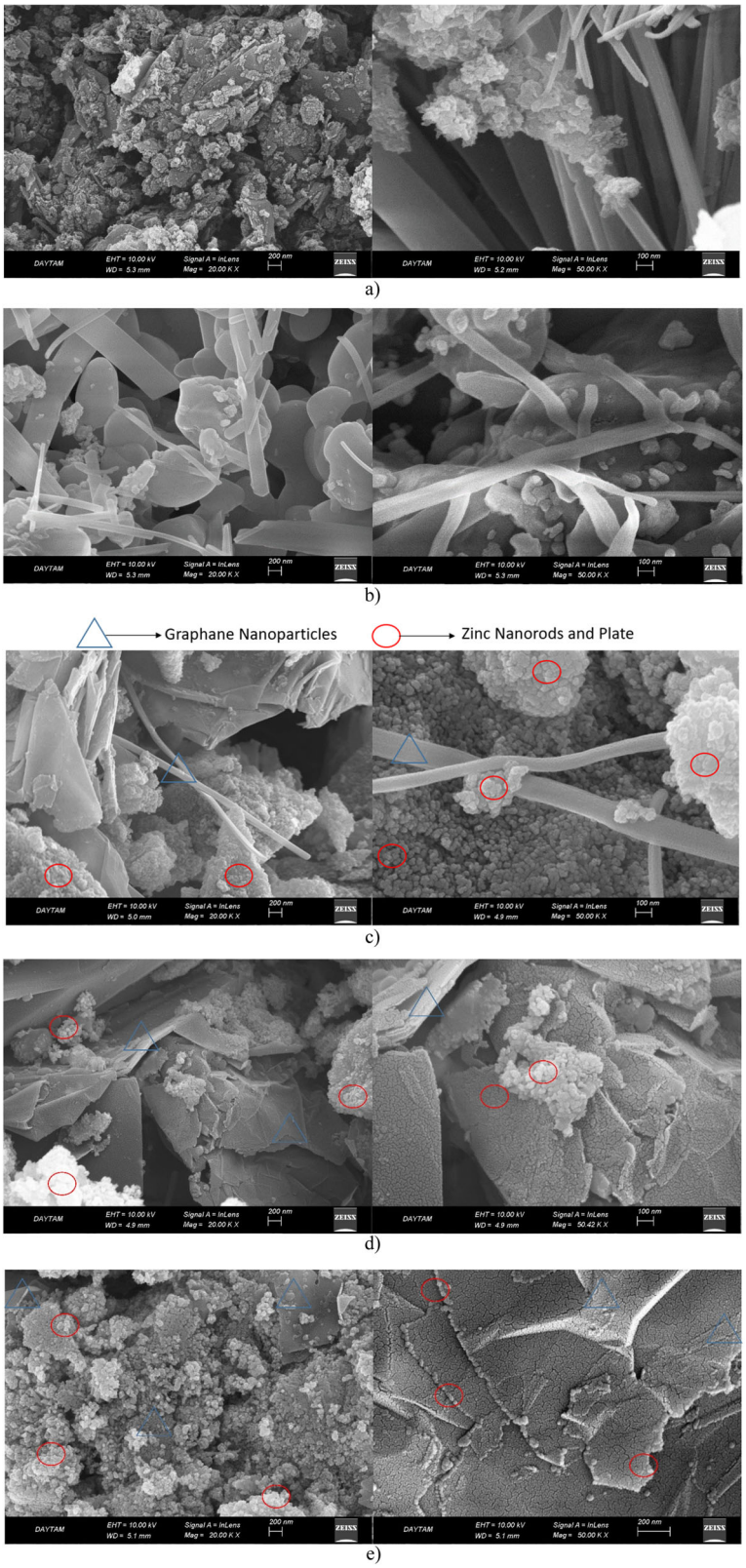

Fig. 5 FE-SEM images of nanoparticles **a** GO, **b** ZnO, **c** ZnO-1GO, **d** ZnO-3GO, **e** ZnO-5GO

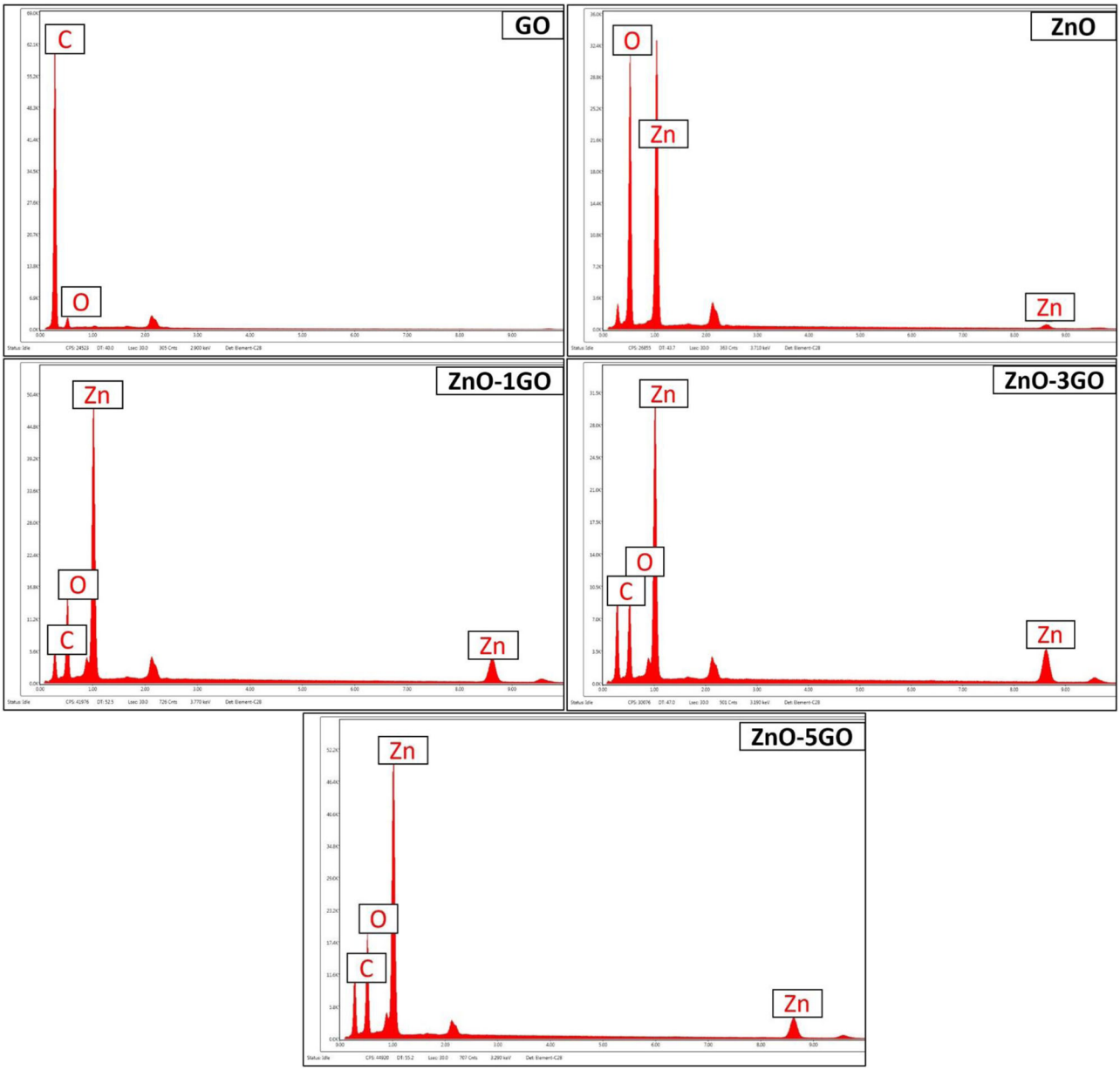

Fig. 6 EDX spectra of nano ZnO

Table 5 EDX analysis results of different sample groups

Sample	Content (Wt.%)		
	Zn	O	C
GO	–	2.90	97.10
ZnO	88.07	11.93	–
ZnO-1GO	79.26	11.46	9.28
ZnO -3GO	71.13	12.99	15.87
ZnO-5GO	64.70	14.89	20.41

Table 6 Dielectric parameters of ZnO-GO composites at 10 kHz at room temperature

Sample	Dielectric constant (ε‘)	Dielectric Loss (ε‘)	AC Conductivity	Log σ_{ac} (S/cm)
GO	172.78	110340.023	9.81×10^{-4}	−3.038
ZnO-5 GO	117.55	75727.291	1.12×10^{-4}	−3.948
ZnO-3 GO	104.98	75443.791	6.75×10^{-5}	−4.170
ZnO-1 GO	27.75	17.322	1.27×10^{-8}	−7.895
ZnO	12.07	0.844	3.43×10^{-8}	−7.464

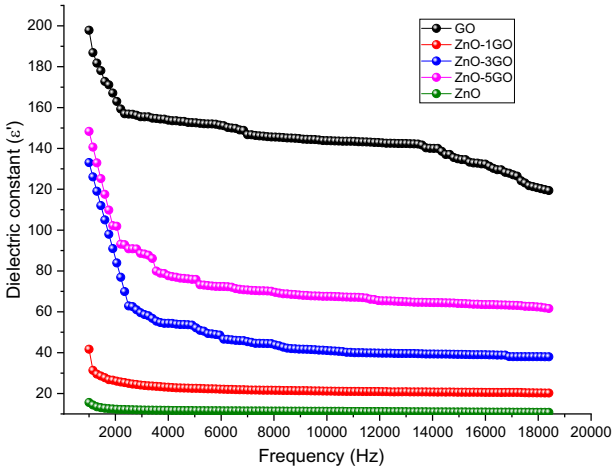

Fig. 7 Dependence of dielectric constant of ZnO/GO composites as a function of frequency

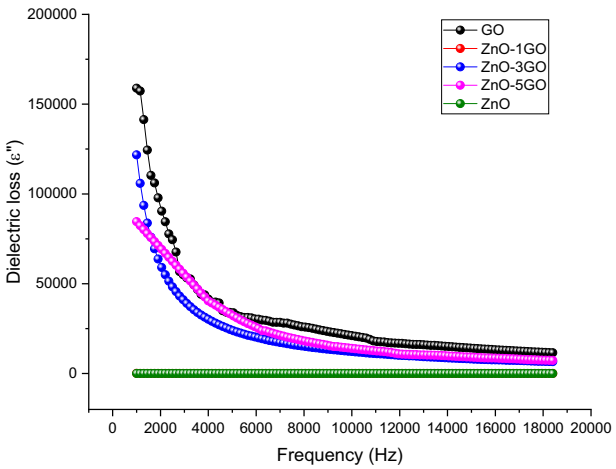

Fig. 8 Dependence of dielectric loss of ZnO/GO composites as a function of frequency

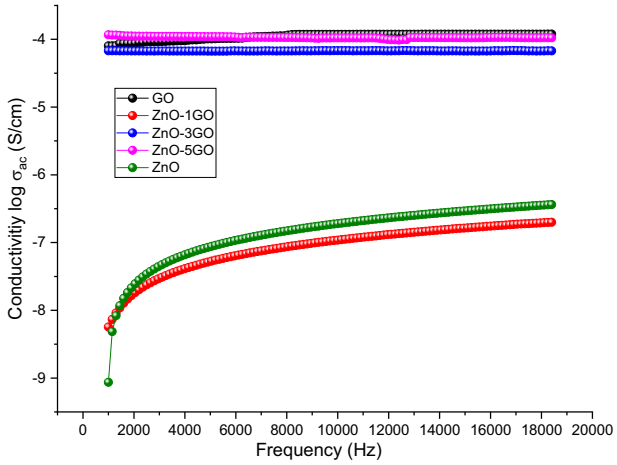

Fig. 9 Dependence of ac conductivity of ZnO/GO composites as a function of frequency

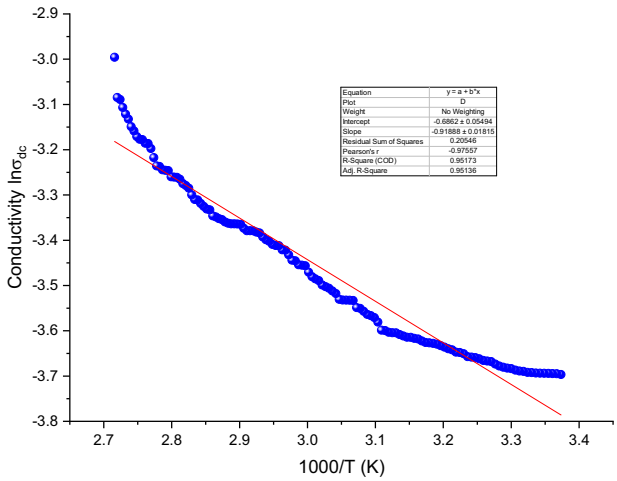

Fig. 10 Temperature dependence of dc conductivity for the ZnO/3GO composite

the orientation of the molecules under the applied field and are connected to the material's structure [63].

Figures 7–9 show the frequency dependent variation curves of dielectric constant (ε‘), dielectric loss (ε“) and (c) ac conductivity of ZnO-GO composites. As seen in Figs. 8 and 9, the values of ε‘ and ε“‘ decrease with increasing frequency. This decrease in the dielectric constant with increasing frequency is a result of the decrease in polarization with increasing frequency. Because of the interfacial polarization, dielectric loss exhibits a tendency to vary at different frequencies [64, 65]. Due to the oxygen functional group present in the GO structure, the addition of different ratios of GO to pure ZnO increased the concentration of oxygen vacancies and charge carriers. This leads to an increase in the interactions between the effects producing dipole moments [66]. The electrical conductivity distribution (σ_{ac}) is an important parameter that gives information about the material. As shown in Fig. 10, σac values increase with increasing frequency. The decrease in polarization with increasing frequency leads to an increase in conductivity with increasing frequency as seen in this graph. Since the number of carriers may increase as a result of the decrease in polarization, there may be an increase in ac conductivity.

Polarization occurs in low-frequency electric fields, with negligible losses. As the frequency rises, it becomes more difficult to match the electric field, and losses cannot be ignored. As the frequency increases, there is no more polarization, and so the dielectric constant rapidly drops [67]. As the frequency rises, the influence of the dipoles grows, polarization occurs, and the dielectric constant falls. This reduction in the dielectric constant suggests that there is surface polarization at that site. When an electric field is applied to a dielectric substance, charges move over its surface [68].

The concentration of filler graphene oxide affected the AC conductivity of ZnO-GO nanocomposites. The ac values of ZnO-GO nanocomposites with 1 wt.%, 3 wt.%, and 5 wt.% graphene oxide were1.27×10^{-8}, 6.75×10^{-5}, and 1.12×10^{-4}, respectively,

As a result, at 3 wt.% graphene oxide, the ZnO-GO nanocomposites' behavior changed from insulating to partly conducting due to the percolation-induced creation of a conductivity network.

The loose clustering of ZnO particles led to a decrease in conductivity. While pure ZnO has a conductivity comparable to or greater than that of a pure composite containing 5 wt. % GO. This may be because the ZnO and GO have a strong interfacial contact, which boosts electronic and dipole polarizations [69].

From ambient temperature to 365 K, the DC conductivities of composites were examined. ZnO-3GO and ZnO-5GO composites dc conductivities varied between 10^{-4} and 10^{-2} S/m, and it can be shown that adding 5 wt.% graphene oxide caused σ_{dc} to rise reasonably. The DC conductivity of composites consisting of ZnO-3GO and ZnO-5GO is shown in Figs. 10 and 11 as a function of temperature. The behavior of the $\ln\sigma_{dc}$ was illustrated in the figure as a function of temperature (1/T). There was a linear association between lns 1000/T and the composites. The Arrhenius formula shown below may be used to express this connection as [70]:

$$\sigma = \sigma_o \exp\left(-\frac{E_a}{k_B T}\right)$$

where T is the temperature, Ea is the activation energy, kB is the Boltzmann constant, and so is the preexponential factor.

The DC electrical conductivity values of ZnO-3GO and ZnO-5GO composites at room temperature were calculated as 5.27×10^{-04} S/cm and 3.65×10^{-02} S/cm, respectively. According to these values, ZnO-3GO and ZnO-5GO composites showed semiconductivity and ZnO/5GO composite has the highest DC electrical conductivity at room temperature. The activation energies of ZnO-3GO and ZnO-5GO were calculated as 0.078 and 0.205 eV, respectively.

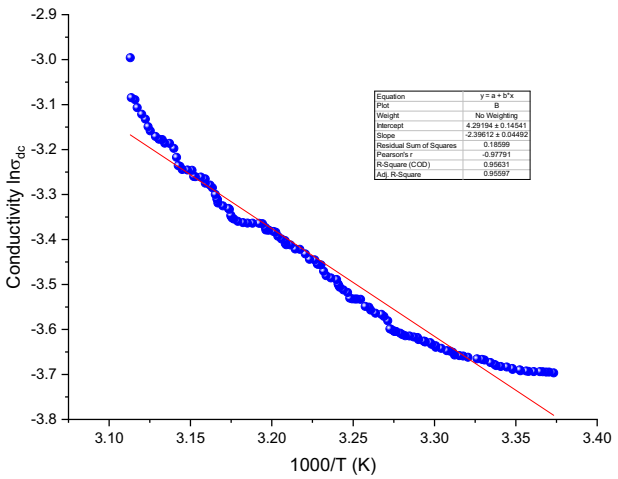

Fig. 11 Temperature dependence of dc conductivity for the ZnO/5GO composites

4 Conclusions

In this study, the synthesis of 1 wt.%, 3 wt.%, and 5 wt.% GO doped ZnO and GO doped ZnO nanoparticles was studied. Sol-gel synthesis was used for successfully synthesizing GO in the nanoscale. The results obtained in the study are summarized below.

- Nanoparticles with great purity and homogeneity were synthesized.
- The XRD peak intensities and positions were found to preserve the distinctive peaks of ZnO and GO.
- As the amount of GO doping in ZnO-GO nanoparticles increased, the diffraction plane shifts and peak intensities also increased.
- According to FE-SEM images, ZnO nanoparticles and GO nanoparticles were homogeneously distributed on the surface of ZnO nanorods and plates. The crystal diameters, unit cell volume and lattice properties of the nanoparticles increased with increasing GO addition.
- The shift in charge centers in nanoparticles is assumed to be the cause of the dielectric constant rising with the amount of GO reinforcement.
- The addition of GO to ZnO nanoparticles improved their dielectric response, and the addition of GO to electrical conductivity had a favorable impact on the ZnO nanoparticles.
- When literature studies were examined, superior findings were obtained based on the dielectric and electrical conductivity values of pure ZnO nanoparticles.
- These findings suggest that the study might be broadened and applied to a number of scenarios. According to data analysis of dielectric constant, loss, and AC conductivity, ZnO-GO nanoparticles could be an important component in the development of solar cells, photovoltaic devices, and semiconductor electronic devices.

Author contributions The study's design was contributed to by all of the writers. CKM and MH were in charge of nanoparticle preparation and characterization. CKM, BT, BA and MH wrote the first draft and general comments on the document. FB contributed to the understanding and interpretation of nanoparticle dielectric characteristics. The submitted version of the article has been read and approved by all authors.

Funding Open access funding provided by the Scientific and Technological Research Council of Türkiye (TÜBİTAK).

Compliance with ethical standards

Conflict of interest The authors declare no competing interests.

Publisher's note Springer Nature remains neutral with regard to jurisdictional claims in published maps and institutional affiliations.

References

1. Nile SH, Baskar V, Selvaraj D, Nile A, Xiao J, Kai G (2020) Nanotechnologies in food science: applications, recent trends, and future perspectives. Nano Micro Lett 12:1–34
2. Gajendiran J, Rajendran V (2014) Synthesis and characterization of coupled semiconductor metal oxide (ZnO/CuO) nanocomposite. Mater Lett 116:311–313
3. Huang X, Qi X, Boey F, Zhang H (2012) Graphene-based composites. Chem Soc Rev 41:666–686
4. Jablan M, Soljačić M, Buljan H (2013) Plasmons in graphene: fundamental properties and potential applications. Proceedings of the IEEE, 101:1689–1704.
5. Jammula RK, Pittala S, Srinath S, Srikanth VVSS (2015) Strong interfacial polarization in ZnO decorated reduced-graphene oxide synthesized by molecular level mixing. Phys Chem Chem Phys 17:17237–17245
6. Zhang L, Yu X, Hu H, Li Y, Wu M, Wang Z et al. (2015) Facile synthesis of iron oxides/reduced graphene oxide composites: application for electromagnetic wave absorption at high temperature. Sci Rep 5:1–9
7. Naidu K, Sarmash T, Maddaiah M, Reddy VN, Subbarao T (2015) Structural and dielectric properties of CuO-doped SrTiO3 ceramics. AIP Conf Proc 1665; 040001
8. Sudhakar YN, Hemant H, Nitinkumar SS, Poornesh P, Selvakumar M (2017) Green synthesis and electrochemical characterization of rGO–CuO nanocomposites for supercapacitor applications. Ion 23:1267–1276
9. Bibi M, Abbas H, Baqi S (2017) Outcome of temperature variation on sol-gel prepared CuO nanostructure properties (optical and dielectric). Mater Chem Phys 192:67–71
10. Fuku X, Kaviyarasu K, Matinise N, Maaza M (2016) Punicalagin green functionalized Cu/Cu 2 O/ZnO/CuO nanocomposite for potential electrochemical transducer and catalyst. Nanoscale Res Lett 11:1–12
11. Poornaprakash B, Chalapathi U, Babu S, Park S-H (2017) Structural, morphological, optical, and magnetic properties of Gd-doped and (Gd, Mn) co-doped ZnO nanoparticles. Phys E Low Dimensional Syst Nanostruct 93:111–115
12. Sidhu GK, Kumar R (2017) Role of anionic and cationic surfactants on the structural and dielectric properties of ZrO2 nanoparticles. Appl Surf Sci 392:598–607
13. Hong R, Pan T, Qian J, Li H (2006) Synthesis and surface modification of ZnO nanoparticles. Chem Eng J 119:71–81
14. Wang ZL (2004) Nanostructures of zinc oxide. Mater Today 7:26–33
15. Serier H, Gaudon M, Menetrier M (2009) Al-doped ZnO powdered materials: Al solubility limit and IR absorption properties. Solid State Sci 11:1192–1197
16. Lotus AF, Kang YC, Walker JI, Ramsier RD, Chase GG (2010) Effect of aluminum oxide doping on the structural, electrical, and optical properties of zinc oxide (AOZO) nanofibers synthesized by electrospinning. Mater Sci Eng B 166:61–66
17. Cheng H, Xu XJ, Hng HH, Ma J (2009) Characterization of Al-doped ZnO thermoelectric materials prepared by RF plasma powder processing and hot press sintering. Ceram Int 35:3067–3072
18. Verma A, Khan F, Kumar D, Kar M, Chakravarty BC, Singh SN et al. (2010) Sol–gel derived aluminum doped zinc oxide for application as anti-reflection coating in terrestrial silicon solar cells. Thin Solid Films 518:2649–2653
19. Zamiri R, Kaushal A, Rebelo A, Ferreira JMF (2014) Er doped ZnO nanoplates: synthesis, optical and dielectric properties. Ceram Int 40:1635–1639
20. Zamiri R, Lemos AF, Reblo A, Ahangar HA, Ferreira JMF (2014) Effects of rare-earth (Er, La and Yb) doping on morphology and structure properties of ZnO nanostructures prepared by wet chemical method. Ceram Int 40:523–529
21. Zamiri R, Zakaria A, Ahangar HA, Darroudi M, Zak AK, Drummen GPC (2012) Aqueous starch as a stabilizer in zinc oxide nanoparticle synthesis via laser ablation. J Alloy Compd 516:41–48
22. Zamiri R, Zakaria A, Jorfi R, Zamiri G, Shokati Mojdehi M, Abbastabar Ahangar H et al. (2013) Laser assisted fabrication of ZnO/Ag and ZnO/Au core/shell nanocomposites. Appl Phys A 111:487–493
23. Zamiri R, Singh BK, Dutta D, Reblo A, Ferreira JMF (2014) Electrical properties of Ag-doped ZnO nano-plates synthesized via wet chemical precipitation method. Ceram Int 40:4471–4477
24. Murray JS, Shields ZP-I, Lane P, Macaveiu L, Bulat FA (2013) The average local ionization energy as a tool for identifying reactive sites on defect-containing model graphene systems. J Mol Model 19:2825–2833
25. Murray JS, Shields ZP, Politzer P (2014) "The Local Ionization Energy as a Guide to Site Reactivities on Graphenes." Design and Applications of Nanomaterials for Sensors. Dordrecht: Springer Netherlands, 249–269.
26. Bagherzadeh M, Farahbakhsh A (2015) Surface functionalization of graphene. Graphene materials: Fundamentals and emerging applications, 25–65.
27. Nieto A, Bisht A, Lahiri D, Zhang C, Agarwal A (2017) Graphene reinforced metal and ceramic matrix composites: a review. Int Mater Rev 62:241–302
28. Li Q, Mahmood N, Zhu J, Hou Y, Sun S (2014) Graphene and its composites with nanoparticles for electrochemical energy applications. Nano Today 9:668–683
29. Atif R, Shyha I, Inam F (2016) Mechanical, thermal, and electrical properties of graphene-epoxy nanocomposites—A review. Polym 8:281
30. Ahmadi N, Nemati A, Bagherzadeh M (2018) Synthesis and properties of Ce-doped TiO2-reduced graphene oxide nanocomposite. J Alloy Compd 742:986–995
31. Ebrahimi Naghani M, Neghabi M, Zadsar M, Abbastabar Ahangar H (2023) Synthesis and characterization of linear/nonlinear optical properties of graphene oxide and reduced graphene oxide-based zinc oxide nanocomposite. Sci Rep 13:1496

32. Karyaoui M, Jemia DBen, Daoudi M, Bardaoui A, Boukhachem A, Amlouk M et al. (2021) Physical properties of graphene oxide GO-doped ZnO thin films for optoelectronic application. Appl Phys A 127:1–14
33. Khan A, Kamal T, Saad M, Ameen F, Bhat SA, Khan MA et al. (2023) Synthesis and antibacterial activity of nanoenhanced conjugate of Ag-doped ZnO nanorods with graphene oxide. Spectrochim Acta Part A Mol Biomol Spectrosc 290:122296
34. Rotte NK, Subbareddy Y, Puttapati SK, Srikanth V, Kaviyarasu K (2023) Morphological features and photoluminescence of ZnO and ZnO decorated S, N-doped few-layered graphene (ZnO–S, N-FLGs). J Phys Chem Solids 174:111175
35. Kumar V, Madan R, Singh B, Mohan D (2023) Room-Temperature acetone gas sensing properties of graphene oxide/zinc oxide nanocomposites synthesized by sol–gel method. J Mater Sci Mater Electron 34:582
36. Raliya R, Tarafdar JC (2013) ZnO nanoparticle biosynthesis and its effect on phosphorous-mobilizing enzyme secretion and gum contents in Clusterbean (Cyamopsis tetragonoloba L.). Agric Res 2:48–57
37. Reda SM (2010) Synthesis of ZnO and Fe2O3 nanoparticles by sol–gel method and their application in dye-sensitized solar cells. Mater Sci Semicond Process 13:417–425
38. Mote VD, Purushotham Y, Dole BN (2016) Structural, morphological, physical and dielectric properties of Mn doped ZnO nanocrystals synthesized by sol–gel method. Mater Des 96:99–105
39. Azizah N, Muhammady S, Purbayanto MAK, Nurfani E, Winata T, Sustini E et al. (2020) Influence of Al doping on the crystal structure, optical properties, and photodetecting performance of ZnO film. Prog Nat Sci Mater Int 30:28–34
40. Zegadi C, Abdelkebir K, Chaumont D, Adnane M, Hamzaoui S (2014) Influence of Sn low doping on the morphological, structural and optical properties of ZnO films deposited by sol gel dip-coating. Adv Mater Phys Chem 4;2014
41. Akhtar MJ, Ahamed M, Kumar S, Khan MAM, Ahmad J, Alrokayan SA (2012) Zinc oxide nanoparticles selectively induce apoptosis in human cancer cells through reactive oxygen species. Int J Nanomedicine 7:845–857
42. Zhou J, Zhao F, Wang Y, Zhang Y, Yang L (2007) Size-controlled synthesis of ZnO nanoparticles and their photoluminescence properties. J Lumin 122:195–197
43. Khoshhesab ZM, Sarfaraz M, Asadabad MA (2011) Preparation of ZnO nanostructures by chemical precipitation method. Synth React Inorg, Met Nano-Met Chem 41:814–819
44. Siburian R, Simanjuntak C, Supeno M, Lumbanraja S, Sihotang H (2018) New route to synthesize of graphene nano sheets. Orient. J. Chem 34:182–187
45. Yasin G, Arif M, Shakeel M, Dun Y, Zuo Y, Khan WQ et al. (2018) Exploring the nickel–graphene nanocomposite coatings for superior corrosion resistance: manipulating the effect of deposition current density on its morphology, mechanical properties, and erosion-corrosion performance. Adv Eng Mater 20:1701166
46. Ahmad A, Ullah S, Khan A, Ahmad W, Khan AU, Khan UA et al. (2020) Graphene oxide selenium nanorod composite as a stable electrode material for energy storage devices. Appl Nanosci 10:1243–1255
47. Labhane PK, Patle LB, Huse VR, Sonawane GH, Sonawane SH (2016) Synthesis of reduced graphene oxide sheets decorated by zinc oxide nanoparticles: crystallographic, optical, morphological and photocatalytic study. Chem Phys Lett 661:13–19
48. Ajinsundar S, Rimal Issac R, Gopalakrishnan S, John N (2019) Studies on new material: carbon dot-graphene oxide-zinc oxide nanocomplex. Materials Science-Poland, https://doi.org/10.2478/msp-2019-0085.
49. Ahmad M, Ahmed E, Ahmed W, Elhissi A, Hong ZL, Khalid NR (2014) Enhancing visible light responsive photocatalytic activity by decorating Mn-doped ZnO nanoparticles on graphene. Ceram Int 40:10085–10097
50. Sahai A, Goswami N (2014) Structural and vibrational properties of ZnO nanoparticles synthesized by the chemical precipitation method. Phys E Low Dimensional Syst Nanostruct 58:130–137
51. Goswami N, Sharma DK (2010) Structural and optical properties of unannealed and annealed ZnO nanoparticles prepared by a chemical precipitation technique. Phys E Low Dimensional Syst Nanostruct 42:1675–1682
52. Sengupta K, Das R, Banerjee G (1992) Measurement of thermal conductivity of refractory bricks by the nonsteady state hot-wire method using differential platinum resistance thermometry. J Test Eval 20:454–459
53. Gul W, Alrobei H (2021) Effect of graphene oxide nanoparticles on the physical and mechanical properties of medium density fiberboard. Polymers 13:1818
54. Emiru TF, Ayele DW (2017) Controlled synthesis, characterization and reduction of graphene oxide: A convenient method for large scale production. Egypt J Basic Appl Sci 4:74–79
55. George A, Sharma SK, Chawla S, Malik MM, Qureshi MS (2011) Detailed of X-ray diffraction and photoluminescence studies of Ce doped ZnO nanocrystals. J Alloy Compd 509:5942–5946
56. Ngo-Duc T, Singh K, Meyyappan M, Oye MM (2012) Vertical ZnO nanowire growth on metal substrates. Nanotechnology 23:194015
57. Chen L-Z, Huang D-D, Ge J-Z, Wang F-M (2013) A novel Ag (I) coordination polymers based on 2-(pyridin-4-yl)-1H-imidazole-4, 5-dicarboxylic acid: Syntheses, structures, ferroelectric, dielectric and optical properties. Inorg Chim Acta 406:95–99
58. Liao W-Q, Zhou Q-Q, Zhang Y (2013) Jin L. Synthesis, structures and dielectric properties of two five-coordinate copper (II) complexes based on N-chloromethyl-1, 4-diazabicyclo [2.2. 2] octane. Inorg Chem Commun 33:161–164
59. Koran K, Özen F, Biryan F, Demirelli K, Görgülü AO (2016) Eu + 3-doped chalcone substituted cyclotriphosphazenes: Synthesis, characterizations, thermal and dielectrical properties. Inorg Chim Acta 450:162–169
60. Fratini S, Morpurgo AF, Ciuchi S (2008) Electron–phonon and electron–electron interactions in organic field effect transistors. J Phys Chem Solids 69:2195–2198
61. Willander M, Yang LL, Wadeasa A, Ali SU, Asif MH, Zhao QX et al. (2009) Zinc oxide nanowires: controlled low temperature growth and some electrochemical and optical nano-devices. J Mater Chem 19:1006–1018
62. Wadaan MA (2023) Zinc oxide doped on reduced graphene oxide nanosheets activated by solar radiation for degradation of organic pollutants and bacterial inactivation. Chemosphere 336:139105
63. Grill A, Patel V (2001) Ultralow-k dielectrics prepared by plasma-enhanced chemical vapor deposition. Appl Phys Lett 79:803–805
64. Rajasekar K, Subbarayan A, Sathyamoorthy R (2006) AC and dielectric properties of thermally evaporated p-type (Sb2Te3) 70 (Bi2Te3) 30 thin films. Sol Energy Mater Sol Cells 90: 2515–2522
65. Karteri I (2017) Determination of Dıelectrıcal Properties of Induced Grapen Oxide Interfacial Layered Metal Oxide Semi-inetchen Capacitor. Nigde Ömer Halisdemir Univ Eng Sci J 6:387–393
66. Ahamad T, Ahmed AS (2023) Influence of graphene oxide on the dielectric properties of biogenically synthesized ZnO nanoparticles. Hybrid Adv 3:100059
67. Dakin TW (2006) Conduction and polarization mechanisms and trends in dielectric. IEEE Electr Insul Mag 22:11–28
68. Buscaglia MT, Viviani M, Buscaglia V, Mitoseriu L, Testino A, Nanni P et al. (2006) High dielectric constant and frozen

macroscopic polarization in dense nanocrystalline Ba Ti O 3 ceramics. Phys Rev B 73:64114
69. Güler Ö, Güler SH, Başgöz Ö, Albayrak MG, Yahia IS (2019) Synthesis and characterization of ZnO-reinforced with graphene nanolayer nanocomposites: electrical conductivity and optical band gap analysis. Mater Res Express 6:95602
70. Torğut G, Biryan F, Demirelli K (2019) Effect of graphite particle fillers on dielectric and conductivity properties of poly (NIPAM-co-HEMA). Bull Mater Sci 42:1–11
71. Prajapati CS, Sahay PP (2013) Influence of In doping on the structural, optical and acetone sensing properties of ZnO nanoparticulate thin films. Mater Sci Semicond Process 16:200–210